AIAA-92-3739

Current-Driven Plasma Acceleration Versus Current-Driven Energy Dissipation

Part III: Anomalous Transport

Edgar Y. Choueiri, Arnold J. Kelly and Robert G. Jahn
Electric Propulsion and Plasma Dynamics Laboratory
Princeton University, Princeton, NJ 08544
USA

AIAA/SAE/ASME/ASEE
28th Joint Propulsion Conference and Exhibit
July 6-8, 1992 / Nashville, TN

Current-Driven Plasma Acceleration Versus Current-Driven Energy Dissipation Part III: Anomalous Transport*

E.Y. Choueiri, A.J. Kelly and R.G. Jahn.

Electric Propulsion and Plasma Dynamics Laboratory
Princeton University, Princeton, NJ 08544, USA

Abstract

In the first two papers of this series, the linear kinetic theory of instabilities in a magnetoactive, collisional, finite-beta, current-carrying and flowing plasma was developed, specialized for the parameters of the MPD thruster and compared to experimental measurements. In the present paper we use the linear stability description of the previous two papers along with weak turbulence theory to develop a second order description of wave-particle transport and anomalous dissipation. The goal is to arrive at anomalous transport coefficients that can be readily included in fluid flow codes. In particular, we derive expressions for the heating rates of ions and electrons by the unstable waves and for the electron-wave momentum exchange rate that controls the anomalous resistivity effect. Comparative calculations were undertaken assuming four different saturation models: ion trapping, electron trapping, ion resonance broadening and thermodynamic bound. A foremost finding is the importance of the role of electron Hall parameter in scaling the level of anomalous dissipation for the parameter range of the MPD thruster plasma. Polynomial expressions of the relevant transport coefficients cast solely in terms of macroscopic parameters are also obtained for inclusion in plasma fluid codes for the self-consistent numerical simulation of real thruster flows including microturbulent effects.

*This work is supported by the National Aeronautics and Space Administration under contract NASA-954997 and by grants from Rocket Research Inc. and DOE/Princeton Plasma Physics Laboratory

1 Introduction

The acceleration process in self-field electromagnetic plasma accelerators is current-driven with the thrust increasing with the square of the total current. It is also known that the current can drive microinstabilities in the plasma which may, through induced microturbulence, substantially increase dissipation and adversely impact the efficiency. The antagonism between current-driven acceleration and current-driven turbulent dissipation has been the subject of a trilogy of papers with the present one being the last. In the first two papers[1, 2], the linear kinetic theory of instabilities in a magnetoactive, collisional, finite-beta, current-carrying and flowing plasma was developed, specialized for the parameters of the MPD thruster and compared to experimental measurements. The presence of current-driven microinstabilities in such accelerator plasmas have been experimentally established in the plasma of the MPD thruster at both low and high power levels[2, 3].

In brief, our previous theoretical studies[2, 4] have identified the dominant mode to be a finite-beta lower hybrid current-driven instability (LHCDI) whereby lower hybrid waves couple with pseudo-whistler waves causing a finite polarization mode to go unstable with considerable disturbance to the magnetic field.

In the present paper we use the linear stability description of the previous two papers along with weak turbulence theory to develop a second order description of wave-particle transport and anomalous dissipation. The goal is to arrive at anomalous transport coefficients that can be readily included in fluid flow codes for practical numerical simulation of real thruster flows including microturbulent effects[5, 6].

In Section 2 we outline the basic formalism we adopt for our formulation of anomalous transport.

In Section 3 we use the statistical description of the previous section to derive general *finite-beta* expressions for the anomalous ion and electron heating rates as well as for the electron-wave momentum exchange rate that controls the anomalous resistivity effect. These expressions are cast as integrals in wavevector space of quantities that depend on the various elements of the linear dispersion tensor derived in Part II of our study[2], on the roots of the linear dispersion relation and on the saturation energy density of the fluctuating (turbulent) fields denoted by $\mathcal{E}_t$.

We then turn our attention in Section 4 to the difficult question of the saturation mechanism that dictates the magnitude and dependencies of $\mathcal{E}_t$. We consider four models for $\mathcal{E}_t$ based on four possible saturation mechanisms.

In Section 5 we show various calculations of the anomalous heating and momentum exchange rates for plasma parameters of interest and compare their magnitudes to classical values.

We finally conclude in Section 6 by using these calculations to arrive at polynomial expressions of the relevant transport coefficients cast solely in terms of macroscopic parameters for inclusion in plasma fluid codes of the accelerator.

2 Weak Turbulence Kinetic Formalism for Anomalous Transport

The kinetic theory of weak turbulence was first developed by *Vedenov, Velikhov and Sagdeev*[7] (1961) as well as *Drummond, Pines and Rosenbluth* [8] (1962). Its current status is probably best exposed by *Galeev and Sagdeev* in ref. [9] (1982). The theory allows for far deeper insight into the description of turbulent transport than that afforded by the hydrodynamic theory of turbulence. This is due to the fact that, unlike a neutral fluid where turbulence is synonymous with strong nonlinear couplings, plasma microturbulence is often characterized by primarily *linear* interactions between unstable modes superimposed on small amplitude nonlinearly induced waves[10, p. 289].

Formally, the validity of the weak turbulence theory hinges on the smallness of the ratio of the fluctuating energy density to the plasma thermal energy density

$$\frac{\mathcal{E}_t}{\sum_s n_s T_s} \ll 1, \tag{1}$$

where n_s and T_s are the density and temperature of species s. We shall find it more convenient in the following sections to deal with the ratio $\mathcal{E}_t/n_0T_i$, (n_0 representing the background charged particle density) which is very close to the above ratio for a quasi-equithermal plasma. It is possible to relate the weak turbulence scaling parameter $\mathcal{E}_t/n_0T_i$ to the experimentally measurable density fluctuation $\tilde{n}/n_0$, where the tilde denotes a fluctuating quantity by noting that $\tilde{n}/n_0 \approx e\tilde{\phi}/T_e$ and $e\tilde{\phi} \approx e\tilde{E}/k$ (where e is the electron charge, $\tilde{\phi}$ the wave potential, k the wavenumber or the magnitude of the wavevector $\boldsymbol{k}$ and E the electric field) so that

$$\frac{\mathcal{E}_t}{n_0T_i} \approx \frac{T_e}{T_i}\frac{(kr_{ce})^2}{4}\left(\frac{\tilde{n}}{n_0}\bigg|_{rms}\right)^2. \tag{2}$$

Experimental evidence of turbulent fluctuations caused by cross-field current-driven instabilities was recently found in the low-power steady-state MPD thruster plasma at various conditions and locations in the plume[11, 3]. These measured turbulent fluctuations had most of their power in the lower hybrid mode with some power appearing sometimes in the electron cyclotron harmonics. Measured values of $(\tilde{n}/n_0)_{rms}$ when such turbulence was observed were on the order of .1 with magnitudes ranging between .05 and .7. For these values, with $1 \geq T_i/T_e \leq 6$, $\mathcal{E}_t = \epsilon_0|\tilde{E}_k|^2/2$ (where ϵ_0 is the permittivity of free space and r_{ce} is the electron cyclotron radius) and assuming $(kr_{ce})^{**} \approx .1$[4], we obtain from Eq. (2) an estimate for $\mathcal{E}_t/n_0T_i$ ranging between 10^{-3} and 10^{-6} implying that the weak turbulence assumption is generally valid.

One of the most fortunate turn of events in modern plasma physics has been the surprising ability of weak turbulence theory to describe experimental observations even for fairly large amplitude waves[10, p. 291]. A historical perspective on the evolution of the formalism is given in [4, pp. 118-119].

2.1 Governing Equations

2.1.1 The Moment-Generating Equation

In this sub-section we present an outline of the derivation of the general form of fluid-like equations governing the evolution of macroscopic quantities under the conditions of weak turbulence. Detailed discussions of such a derivation have already been presented in numerous articles (see refs. [12, 13], for instance, for a tutorial review). We do this in preparation to our

derivation of anomalous transport presented in the following sections.

We should mention at the outset that our interest lies not in the evolution equation itself but rather in its use as a moment-generating equation. Therefore, for the sake of simplicity and in order to keep a connection with the literature, we shall neglect collisions in the kinetic evolution equation. The effects of collisions will be reintroduced later when we use the explicit form of the dispersion tensor elements.

The underlying idea is to consider the distribution function of the s species, f_s, as the sum of a slowly varying ensemble-average part and a rapidly varying fluctuating part

$$f_s(\boldsymbol{x},\boldsymbol{v},t) = F_s(\boldsymbol{v},t) + \tilde{f}_s(\boldsymbol{x},\boldsymbol{v},t) \tag{3}$$

where $F_s(\boldsymbol{v},t) = \langle f_s(\boldsymbol{x},\boldsymbol{v},t)\rangle$ and $\langle\quad\rangle$ denotes an ensemble-average[14] while the tilde denotes a quantity fluctuating due to the effects of unstable waves. When similar partitions are effected on the electric and magnetic field vectors, the kinetic (Vlasov) equation for a spatially uniform equilibrium yields

$$\begin{aligned}\frac{\partial F_s}{\partial t} - \omega_{cs}\frac{\partial F_s}{\partial \phi} + \frac{q_s}{m_s}\left[\tilde{\boldsymbol{E}} + \boldsymbol{v}\times\tilde{\boldsymbol{B}}\right]\cdot\nabla_v F_s = \\ -\left(\frac{\partial \tilde{f}_s}{\partial t} + \boldsymbol{v}\cdot\nabla\tilde{f}_s - \omega_{cs}\frac{\partial \tilde{f}_s}{\partial\phi}\right. \\ \left. + \frac{q_s}{m_s}\left[\tilde{\boldsymbol{E}} + \boldsymbol{v}\times\tilde{\boldsymbol{B}}\right]\cdot\nabla_v\tilde{f}_s\right)\end{aligned} \tag{4}$$

where q_s, m_s, ω_{cs} are charge, mass and cyclotron frequency of species s and where, like in Part II of our study[2], we have chosen to work with the cylindrical phase space coordinates $v_\perp, \phi, v_z$ (representing the velocity perpendicular to the magnetic field $\boldsymbol{B}$, the cylindrical angle and the parallel velocity, the magnetic field being aligned with the z-axis). Taking the ensemble-average of the above equation, while noting that $\langle\tilde{f}_s\rangle = 0$, results in

$$\frac{\partial F_s}{\partial t} - \omega_{cs}\frac{\partial F_s}{\partial\phi} = \left(\frac{\partial F_s}{\partial t}\right)_{AN} \tag{5}$$

where the right hand side represents the anomalous contribution that is the response of the average distribution function to the microturbulent fluctuations and can be written explicitly as

$$\left(\frac{\partial F_s}{\partial t}\right)_{AN} = \left\langle -\frac{q_s}{m_s}\left[\tilde{\boldsymbol{E}} + \boldsymbol{v}\times\tilde{\boldsymbol{B}}\right]\cdot\nabla_v\tilde{f}_s\right\rangle. \tag{6}$$

By subtracting Eq. (6) from Eq. (4) and, in the spirit of weak turbulence theory, neglecting all terms that are quadratic in the fluctuation amplitude (which is tantamount to the neglect of *nonlinear* wave-particle and wave-wave interactions) the following governing equation is obtained for a weakly turbulent plasma

$$\frac{\partial\tilde{f}_s}{\partial t} + \boldsymbol{v}\cdot\nabla\tilde{f}_s - \omega_{cs}\frac{\partial\tilde{f}_s}{\partial\phi} = -\frac{q_s}{m_s}\left[\tilde{\boldsymbol{E}} + \boldsymbol{v}\times\tilde{\boldsymbol{B}}\right]\cdot\nabla_v F_s. \tag{7}$$

The standard procedure in weak turbulence theory (expounded in ref. [14] for instance) is to solve Eq. (7) along with Maxwell's equations for $\tilde{\boldsymbol{E}}, \tilde{\boldsymbol{B}}$ and $\tilde{f}_s$ then substitute the result into Eq. (5) to obtain the evolution of F_s in the presence of microturbulence. We shall not, however, need to do all that for our particular problem of deriving expressions for the momentum and energy exchange rates. Such expressions can be arrived at by taking moments of the governing equation (Eq. (5)) as outlined below.

2.1.2 Evolution of Average Macroscopic Properties under Microturbulence

To obtain the macroscopic evolution equations we take moments of Eq. (5) *i.e.* we multiply the equation by the generic quantity of transport Θ (which could represent mass, momentum or energy) and integrate over velocity space to get

$$\begin{aligned}\frac{\partial}{\partial t}\int\Theta F_s d\boldsymbol{v} - q_s m_s\int(\boldsymbol{v}\times\boldsymbol{B}_0\cdot\nabla_v\Theta)F_s d\boldsymbol{v} = \\ \frac{q_s}{m_s}\left\langle\int\left[\left(\tilde{\boldsymbol{E}} + \boldsymbol{v}\times\tilde{\boldsymbol{B}}\right)\cdot\nabla_v\Theta\right]\tilde{f}_s d\boldsymbol{v}\right\rangle\end{aligned} \tag{8}$$

where we have used integration by parts in order to move the distribution functions outside the operators. Taking successive moments of Eq. (5) is equivalent to substituting $\Theta = 1, \boldsymbol{v}, \boldsymbol{vv}$ (for mass, momentum and energy respectively) in Eq. (8) and integrating over $\boldsymbol{v}$-space. This yields

$$\frac{\partial\langle n_s\rangle}{\partial t} = 0 \tag{9}$$

$$\begin{aligned}\frac{\partial\langle\boldsymbol{\Gamma}_s\rangle}{\partial t} + (\omega_{cs}\boldsymbol{e}_z)\times\langle\boldsymbol{\Gamma}_s\rangle = \\ \frac{q_s}{m_s}\left\langle\tilde{\boldsymbol{E}}\tilde{n}_s + \tilde{\boldsymbol{\Gamma}}_s\times\tilde{\boldsymbol{B}}\right\rangle\end{aligned} \tag{10}$$

$$\begin{aligned}\frac{\partial\langle\boldsymbol{W}_s\rangle}{\partial t} + 2(\omega_{cs}\boldsymbol{e}_z)\times\langle\boldsymbol{W}_s\rangle = \\ 2\frac{q_s}{m_s}\left\langle\tilde{\boldsymbol{E}}\tilde{\boldsymbol{\Gamma}}_s + \tilde{\boldsymbol{W}}_s\times\tilde{\boldsymbol{B}}\right\rangle\end{aligned} \tag{11}$$

where $\boldsymbol{e}_z$ is the unit vector along the z-axis, and we have used the following definitions

$$n_s = \int f_s d\boldsymbol{v} \tag{12}$$

$$\Gamma_s = n_s v_{ds} = \int v f_s \, dv \tag{13}$$

$$W_s = m_s \int v v f_s \, dv \tag{14}$$

for the average number density, the particle flux density and the kinetic energy density tensor, respectively (with v_{ds} as the drift velocity vector of species s).

3 Momentum Exchange and Heating Rates

We now proceed to define and derive explicit relations for the anomalous rates of interest.

The right hand side of Eq. (10) represents the rate of momentum exchange $(\partial \boldsymbol{P}_s/\partial t)_{AN}$ (where the momentum density vector is $\boldsymbol{P}_s = m_s \boldsymbol{\Gamma}_s$) between the particles and the fluctuating fields. Since we shall be interested in the momentum exchange along the drift velocity vector, we write

$$\left(\frac{\partial \boldsymbol{P}_s}{\partial t}\right)_{AN} \cdot \boldsymbol{v}_{ds} = -\left(\nu_s^p\right)_{AN} \boldsymbol{P}_s \cdot \boldsymbol{v}_{ds} \tag{15}$$

where we have defined $(\nu_s^p)_{AN}$ as the effective anomalous momentum exchange rate (or frequency) between species s and the fluctuating fields. Using the explicit expression for $(\partial \boldsymbol{P}_s/\partial t)_{AN}$ from Eq. (10) in the above equation we obtain

$$\left(\nu_s^p\right)_{AN} = -\frac{q_s}{n_s m_s v_{ds}} \left\langle \frac{\tilde{\boldsymbol{E}} \cdot \boldsymbol{v}_{ds} \tilde{n}_s}{v_{ds}} + \frac{\boldsymbol{v}_{ds} \cdot (\tilde{\boldsymbol{\Gamma}}_s \times \tilde{\boldsymbol{B}})}{v_{ds}} \right\rangle \tag{16}$$

where, unlike most derivations in the literature, we are retaining the full electromagnetic character of the microturbulence.

We now specialize the above expression for our particular problem according to the MPD thruster configuration shown in Fig. (1). We thus obtain the effective anomalous momentum exchange rate for electrons along the current after setting $s = e$, staying in the ion reference frame and aligning the relative drift u_{de} along the y-axis,

$$\left(\nu_e^p\right)_{AN} = \frac{e}{n_0 m_e u_{de}} \left\langle \tilde{E}_y \tilde{n}_e + n_0 \tilde{u}_{de_z} \tilde{B}_x - n_0 \tilde{u}_{de_x} \tilde{B}_z \right\rangle \tag{17}$$

where we have used the relation $\tilde{\boldsymbol{\Gamma}}_s = \tilde{n}_s \boldsymbol{v}_{ds} + n_0 \tilde{\boldsymbol{v}}_{ds}$.

The frequency $(\nu_e^p)_{AN}$ can be thought of as an effective "collision" frequency between the electrons and the fluctuating fields and can thus be associated with a resistivity called "anomalous resistivity" the same way that the coulomb collision frequency ν_{ei} is associated with the classical Spitzer resistivity. By analogy the anomalous resistivity $(\eta)_{AN}$ is proportional to $(\nu_e^p)_{AN}$ and is given by

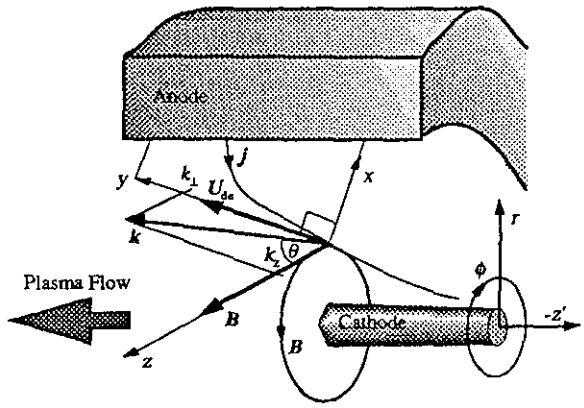

Figure 1: The vectors j, B, k and u_{de} in the local cartesian coordinate frame. Also shown is the accelerator's fixed cylindrical coordinate frame, r-z'-θ.

$$(\eta)_{AN} = \frac{m_e \left(\nu_e^p\right)_{AN}}{n_0 e^2}. \tag{18}$$

The effective collision frequency $(\nu_e^p)_{AN}$ is therefore a direct measure of anomalous resistivity.

Similarly, for the temperature

$$T_s = \frac{m_s}{3 n_s} \int (v - v_{ds})^2 f_s \, dv \tag{19}$$

we define a heating rate for species s by

$$\nu_s^T \equiv \frac{1}{T_s} \frac{\partial T_s}{\partial t} \tag{20}$$

and obtain, after combining Eqs. (10) and (11) and specializing for the MPD thruster configuration,

$$\left(\nu_i^T\right)_{AN} = \frac{2e}{3 n_0 T_i} \left\langle n_0 \tilde{E} \cdot \tilde{u}_{di} \right\rangle \tag{21}$$

for the ions and

$$\begin{aligned} \left(\nu_e^T\right)_{AN} &= \frac{-2e}{3 n_0 T_e} \left\langle n_0 \tilde{E} \cdot \tilde{u}_{de} \right. \\ &- \left. n_0 u_{de} \left(\tilde{u}_{de_z} \tilde{B}_x - \tilde{u}_{de_x} \tilde{B}_z \right) \right\rangle \end{aligned} \tag{22}$$

for the electrons.

Eqs. (17), (21) and (22) will be the focus of our remaining analysis and calculations.

In order to proceed with more useful forms for these expressions we need to eliminate the fluctuating density, velocity and magnetic field in favor of the fluctuating electric field. For this purpose we invoke, in the spirit of a quasilinear description, relations between the fluctuating quantities and the fluctuating electric field that follow those of their linearly oscillating counterparts. From a generalized Ohm's law we can write for species s[2]

$$\tilde{\boldsymbol{j}}_{s_k} = -i\epsilon_0\omega \boldsymbol{R}^{(s)}\tilde{\boldsymbol{E}}_k \tag{23}$$

(where $\boldsymbol{j}$ is the current density, $\boldsymbol{R}^{(s)}$ is the dispersion tensor of species s and ω is the wave frequency) which, combined with the continuity relation[2]

$$n_s^{(1)} = \frac{\boldsymbol{k}\cdot\boldsymbol{j}_s^{(1)}}{\omega q_s}, \tag{24}$$

gives a useful expression for the fluctuating density of species s

$$\tilde{n}_{s_k} = \frac{\boldsymbol{k}\cdot\tilde{\boldsymbol{j}}_s}{\omega q_s} = -i\frac{\epsilon_0}{q_s}\sum_l k_l \sum_m R_{lm}^{(s)}\tilde{E}_{m_k} \tag{25}$$

where the subscript k is a reminder that these relations are for the spectrally resolved (*i.e.* Fourier transformed) fluctuations. In this expression, $R_{lm}^{(s)}$ are the elements of the tensor representing the dielectric response of species s and can be readily obtained from Eqs. (87)-(94) (derived in Part II of our study[2] and quoted in the appendix) through transformations that will be described further below.

In a similar fashion we can derive an expression for $\tilde{u}_{ds}$ from the following relation

$$\tilde{\boldsymbol{j}}_s = q_s\left(n_0\tilde{\boldsymbol{u}}_{ds} + \tilde{n}_s\boldsymbol{u}_{ds}\right) \tag{26}$$

and Eq. (25), yielding

$$\tilde{\boldsymbol{u}}_{s_k} = -\frac{i\epsilon_0\omega\boldsymbol{R}^{(s)}\tilde{\boldsymbol{E}}_k}{q_s n_0} + \left[i\frac{\epsilon_o}{q_s n_0}\boldsymbol{k}\cdot\left(\boldsymbol{R}^{(s)}\tilde{\boldsymbol{E}}_k\right)\right]\boldsymbol{u}_{ds}. \tag{27}$$

We shall not need to worry about the second term on the right hand side of the above equation in the context of the MPD thruster configuration shown in Fig. (1), because this term vanishes for the ions ($\boldsymbol{u}_{di} = 0$, having chosen to stay in the ion rest frame) and for the electrons it is also nil for the components that figure in Eqs. (17) and (22) (*i.e.* the x and z components) so that we are left with

$$\tilde{u}_{ds_{l_k}} = -i\frac{\epsilon_o}{q_s n_0}\omega\sum_m R_{lm}^{(s)}\tilde{E}_{m_k} \tag{28}$$

where $l = x, z$ for $s = e$; and $l = x, y, z$ for $s = i$.

Having related the fluctuating density and velocity to the fluctuating electric field we need to do the same for $\tilde{\boldsymbol{B}}$. To this end, the following equation

$$\tilde{\boldsymbol{E}} = i\omega\tilde{\boldsymbol{A}} - i\boldsymbol{k}\tilde{\Phi}, \tag{29}$$

which relates the electromagnetic potential $\tilde{\boldsymbol{A}}$ and electrostatic potential $\tilde{\Phi}$ to the electric field $\tilde{\boldsymbol{E}}$ (see Part II of our study[2]), gives, for our particular configuration,

$$\tilde{E}_{x_k} = i\omega\tilde{A}_{x_k} \tag{30}$$

$$\tilde{E}_{y_k} = -ik_\perp\tilde{\Phi}_k - i\omega\frac{k_z}{k_\perp}\tilde{A}_{x_k} \tag{31}$$

$$\tilde{E}_{z_k} = -ik_z\tilde{\Phi}_k + i\omega\tilde{A}_{z_k} \tag{32}$$

Furthermore, combining the above equations with the definition of the electromagnetic potential,

$$\boldsymbol{B} = \nabla\times\boldsymbol{A}, \tag{33}$$

and Coulomb's gauge, yields the desired relations

$$\tilde{B}_{x_k} = \frac{1}{\omega}\left(k_\perp\tilde{E}_{z_k} - k_z\tilde{E}_{y_k}\right) \tag{34}$$

$$\tilde{B}_{y_k} = \frac{k_z}{\omega}\tilde{E}_{x_k} \tag{35}$$

$$\tilde{B}_{z_k} = -\frac{k_\perp}{\omega}\tilde{E}_{x_k}. \tag{36}$$

We are now in a position to evaluate the terms of Eqs. (17), (22) and (21) by carrying the ensemble-averages using the random phase approximation (which is a standard technique of statistical physics commonly used in the spectral resolution of fluctuations, see Ref. [15, pages 371–373] for instance). For the first term in Eq. (17) using Eq. (25) we have,

$$\left\langle\tilde{E}_y\tilde{n}_e\right\rangle = \left\langle\int\int\frac{i\epsilon_0}{e}\sum_l k_l\sum R_{lm}^{(e)} \times\tilde{E}_{m_k}\tilde{E}_{y'_k}e^{i(\boldsymbol{k}\cdot\boldsymbol{x}+\boldsymbol{k}'\cdot\boldsymbol{x})}\,d\boldsymbol{k}\,d\boldsymbol{k}'\right\rangle \tag{37}$$

which yields under the assumption of random phase[1]

$$\left\langle\tilde{E}_y\tilde{n}_e\right\rangle = -\frac{\epsilon_0}{e}\int\Im\left\{\sum_l k_l\sum_m R_{lm}^{(e)}\tilde{E}_m\tilde{E}_y\right\}d\boldsymbol{k} \tag{38}$$

where $\Im\{\ \}$ denotes the imaginary part of a complex quantity. Similarly, we find for the other two terms

[1] From here on, we shall, for the sake of simplicity, drop the subscript k from the fluctuating quantities.

in Eq. (17)

$$\left\langle \tilde{u}_{de_x} \tilde{B}_x \right\rangle = -\frac{\epsilon_0}{e} \int \Im \left\{ \left(\sum_m R^{(e)}_{xm} \tilde{E}_m \right) \times \left(k_\perp \tilde{E}_z - k_z \tilde{E}_y \right) \right\} dk \quad (39)$$

$$\left\langle \tilde{u}_{de_z} \tilde{B}_z \right\rangle = \frac{\epsilon_0}{e} \int \Im \left\{ \left(\sum_m R^{(e)}_{zm} \tilde{E}_m \right) \times k_\perp \tilde{E}_x \right\} dk. \quad (40)$$

If we now substitute the above three equations in Eq. (17), expand and collect the terms in the summations while taking advantage of the following symmetry properties of the dispersion tensor

$$R^{(s)}_{xy} = -R^{(s)}_{xy}; \quad R^{(s)}_{xz} = -R^{(s)}_{xz}; \quad R^{(s)}_{yz} = R^{(s)}_{zy}, \quad (41)$$

we arrive at

$$(\nu^p_e)_{AN} = -\frac{\epsilon_0}{u_{de} m_e n_e} \times \int \Im \left\{ k_\perp \left[\left(\sum_l R^{(e)}_{ll} |\tilde{E}_l|^2 \right) + 2R^{(e)}_{yz} |\tilde{E}_y \tilde{E}_z| \right] \right\} dk. \quad (42)$$

We shall find it convenient, for our particular instability, to cast the the above expression in terms of the spectrally resolved fluctuating field energy density in the perpendicular direction, $\mathcal{E}_{k_\perp}$. This can be done by using the following relations obtained from Eq. (41) and the governing equation[2]

$$\boldsymbol{R}\boldsymbol{E}^{(1)} = 0 \quad (43)$$

(where the superscript denotes the oscillating part of the electric field) to yield

$$A \equiv \frac{\tilde{E}_x}{\tilde{E}_y} = \frac{R_{yy}R_{xz} - R_{xy}R_{yz}}{R_{xy}R_{xz} + R_{xx}R_{yz}} \quad (44)$$

$$B \equiv \frac{\tilde{E}_z}{\tilde{E}_y} = -\frac{R_{xy}R_{xz} - R_{xx}R_{yz}}{R_{xx}R_{xz} + R_{xx}R_{xz}} \quad (45)$$

(where each element R_{lm} is the sum of the corresponding contributions from the electrons, ions and vacuum) to eliminate $\tilde{E}_x$ and $\tilde{E}_z$ and give

$$(\nu^p_e)_{AN} = -\frac{2}{u_{de} m_e n_e} \int \mathcal{E}_{k_\perp} k_\perp \times \Im \left\{ R^{(e)}_{xx} A^2 + R^{(e)}_{yy} + R^{(e)}_{zz} B^2 + 2R^{(e)}_{yz} B \right\} dk. \quad (46)$$

We have carried out our derivation above under the electric field formalism where the relevant dispersion tensor is $\boldsymbol{R}$ (*cf* Eq. (43)). The dispersion tensor $\boldsymbol{D}$ that we derived explicitly in Part II of our study[2], however, was obtained under the potential formalism (*cf* Eqn. (30) of Part II). As was the case in that paper, switching to the potential formalism has some advantages. In the context of anomalous transport, the potential formalism allows a more physical insight by expressing the momentum exchange and heating rates in terms of an electrostatic contribution plus a finite-beta correction. The results obtained so far can readily be recast in terms of the elements D_{lm} of Eqs. (87)-(94), through the following linear transformations obtained from combining Eqs. (43), (30), (31) and (32),

$$R_{xx} = D_{22} \quad (47)$$

$$R_{xy} = -R_{yx} = \frac{k_\perp}{k} \left(\frac{k_z}{k} D_{23} - D_{12} \right) \quad (48)$$

$$R_{xz} = -R_{zx} = -\frac{k^2_\perp}{k^2} D_{23} - \frac{k_z}{k} D_{12} \quad (49)$$

$$R_{yy} = \frac{k^2_\perp}{k^2} \left(D_{11} + 2\frac{k_z}{k} D_{13} \right) + \frac{k^2_z}{k^2} D_{33} \quad (50)$$

$$R_{yz} = R_{yz} = \frac{k_\perp}{k} \left[\frac{k^2_z}{k^2} - \frac{k^2_\perp}{k^2} \right] D_{13} + \frac{k_\perp k_z}{k^2} (D_{11} - D_{33}) \quad (51)$$

$$R_{zz} = \frac{k^2_\perp}{k^2} D_{33} + \frac{k^2_z}{k^2} D_{11} - 2\frac{k^2_\perp}{k^2} \frac{k_z}{k} D_{13}. \quad (52)$$

We also need to separate the contributions of electrons, ions and vacuum in the dispersion tensor, which can be done following

$$D^{(e)}_{lm} = D_{lm} - D^{(0)}_{lm} - D^{(i)}_{lm} \quad (53)$$

where subscripts l and m cover the indices 1, 2 and 3 and where the superscript (0) denotes the contribution of vacuum. The elements $D^{(0)}_{lm}$ and $D^{(i)}_{lm}$ are given by

$$D^{(0)}_{11} = 1, \quad D^{(0)}_{22} = D^{(0)}_{33} = 1 - N^2$$
$$D^{(0)}_{12} = D^{(0)}_{13} = D^{(0)}_{23} = 0 \quad (54)$$

and

$$D^{(i)}_{11} = \frac{2\omega^2_{pi}}{k^2 v^2_{ti}} (1 + \zeta_i Z_i) \quad (55)$$

$$D^{(i)}_{22} = D^{(i)}_{33} = \frac{\omega^2_{pi}}{\omega^2} \zeta_i Z_i \quad (56)$$

$$D^{(i)}_{12} = D^{(i)}_{13} = D^{(i)}_{23} = 0. \quad (57)$$

When the above transformations (Eqs. (47)-(57)) are used in Eq. (46) to eliminate $R^{(e)}_{lm}$ in favor of $D^{(e)}_{lm}$, we finally obtain after some straightforward algebra

$$
\begin{aligned}
(\nu^p_e)_{AN} &= [(\nu^p_e)_{AN}]_L - \frac{2}{u_{de} m_e n_e} \int \mathcal{E}_{k_\perp} k_\perp \\
&\times \Im \left\{ D^{(e)}_{11} \left[B^2 \frac{k_z^2}{k^2} - \frac{k_z^2}{k^2} + 2B \frac{k_\perp k_z}{k^2} \right] \right. \\
&+ D^{(e)}_{22} A^2 + D^{(e)}_{33} \left[\frac{k_z^2}{k^2} + \frac{k_\perp^2}{k^2} B^2 - 2B \frac{k_\perp k_z}{k^2} \right] \\
&+ 2 D^{(e)}_{13} \left[B \frac{k_\perp}{k} \left(\frac{k_z^2}{k^2} - \frac{k_\perp^2}{k^2} \right) \right. \\
&\left. \left. - \frac{k_\perp^2 k_z^2}{k^4} B^2 + \frac{k_\perp^2 k_z}{k^3} \right] \right\} dk \qquad (58)
\end{aligned}
$$

where $[(\nu^p_e)_{AN}]_L$ is the well-known electrostatic (longitudinal) contribution to the anomalous electron momentum exchange rate

$$
[(\nu^p_e)_{AN}]_L = -\frac{2}{u_{de} m_e n_e} \int \mathcal{E}_{k_\perp} k_\perp \Im\{\chi_e\} \, dk \qquad (59)
$$

and $\chi_e = D^{(e)}_{11}$ is the electrostatic susceptibility of the electrons. In the electrostatic limit ($\beta \to 0$) it can be verified that the integrand in Eq. (58) vanishes so that we are left with $(\nu^p_e)_{AN} \to [(\nu^p_e)_{AN}]_L$ and

$$
\Im\{\chi_e\} = \Im\{D^{(e)}_{11}\} = \Im\{-D^{(i)}_{11}\} = \Im\{-\chi_i\}. \qquad (60)
$$

We shall demonstrate through the calculations of Section 5 that the transverse (electromagnetic) or finite-beta correction to $(\nu^e_p)_{AN}$ in Eq. (58) can be substantial, especially for a finite-beta plasma like that of the MPD thruster.

Equations (46) and (58) are equivalent but, for the present analytical discussion, we prefer, from here on to use the former (*i.e.* the electric field formalism) because the resulting expressions are more compact. For our numerical calculations we shall apply the transformations in Eqs. (47) to Eq. (57) in order to obtain the $\boldsymbol{R}$ tensor from the $\boldsymbol{D}$ derived in Part II of our study[2] and quoted here in the appendix.

It is convenient to express $(\nu^p_e)_{AN}$ in units of a natural frequency. We choose, as we did in Part II, the lower hybrid frequency, ω_{lh}, and normalize Eq. (46) to get

$$
\begin{aligned}
\frac{(\nu^p_e)_{AN}}{\omega_{lh}} &= -\frac{v_{ti}}{u_{de}} \left(\frac{T_i}{T_e} \right)^{1/2} \frac{m_i}{m_e} \int \frac{\mathcal{E}_{k_\perp}}{n_0 T_i} \\
&\times \Im \left\{ k_\perp r_{ce} \left[R^{(e)}_{xx} A^2 + R^{(e)}_{yy} \right. \right. \\
&\left. \left. + R^{(e)}_{zz} B^2 + 2 R^{(e)}_{yz} B \right] \right\} d\,k. \qquad (61)
\end{aligned}
$$

We have focused, above, on the anomalous electron momentum exchange rate. Similar derivations, with no conceptual difference, start from Eqs. (21) and (27) and lead to the following expressions for the ion and electron heating rates $\left(\nu^T_i\right)_{AN}$ and $\left(\nu^T_e\right)_{AN}$

$$
\begin{aligned}
\frac{\left(\nu^T_i\right)_{AN}}{\omega_{lh}} &= \frac{4}{3} \int \frac{\mathcal{E}_{k_\perp}}{n_0 T_i} \Im \left\{ \frac{\omega}{\omega_{lh}} \left[R^{(i)}_{xx} A^2 \right. \right. \\
&\left. \left. + R^{(i)}_{yy} + R^{(i)}_{zz} B^2 + 2 R^{(i)}_{yz} B \right] \right\} d\,k \qquad (62) \\
\frac{\left(\nu^T_e\right)_{AN}}{\omega_{lh}} &= \frac{4}{3} \frac{T_i}{T_e} \int \frac{\mathcal{E}_{k_\perp}}{n_0 T_i} \\
&\times \Im \left\{ \left[\frac{\omega}{\omega_{lh}} - k_\perp r_{ce} \left(\frac{T_i}{T_e} \right)^{1/2} \frac{u_{de}}{v_{ti}} \right] \right. \\
&\times \left[R^{(e)}_{xx} A^2 + R^{(e)}_{yz} B + R^{(e)}_{zz} B^2 \right] \\
&+ \frac{k_z}{k} \frac{u_{de}}{v_{ti}} k_\perp r_{ce} \left(\frac{T_i}{T_e} \right)^{1/2} \\
&\times \left[R^{(e)}_{xx} A + R^{(e)}_{xy} + R^{(e)}_{zz} B \right] \\
&+ \frac{\omega}{\omega_{lh}} \left[R^{(e)}_{yy} + R^{(e)}_{yz} B \right] \\
&\left. - A k_\perp r_{ce} \left(\frac{T_i}{T_e} \right)^{1/2} \frac{u_{de}}{v_{ti}} R^{(e)}_{xy} \right\} d\,k. \qquad (63)
\end{aligned}
$$

The above three equations are the sought expressions for our analysis of anomalous transport[2].

4 Saturation Mechanisms

For the numerical analysis of anomalous transport in the MPD thruster plasma, the above three equations, along with the tensor elements in Eqs. (87)-(94), the linear dispersion relation

$$
\det |R_{ij}(\omega, k)| = 0 \qquad (64)
$$

and the transformations in Eqs. (47)-(57) form an *almost* complete set of equations in terms of the fol-

[2] *Winske et al.*[16] (1985) have derived expressions for the anomalous heating rates of ions and electrons in finite-beta plasmas. *Their expressions differ from ours because of a difference* in evaluating the ensemble-averages. In going from Eq. (37) to Eq. (38) above, for instance, these authors would neglect in the summation the cross-terms $\tilde{E}_l \tilde{E}_m$ with $l \neq m$ (see Equations (14) and (15) of that paper). *There does not seem to be, however,* a valid *a priori* reason to neglect such cross-terms[17]. Indeed, had we dropped these terms, the last term of the sum in the integrand of Eq. (46) would vanish. This term, $2R^{(e)}_{zz} B^2$, was found to be important for many situations we have investigated numerically. Furthermore, had we dropped the cross-terms it would not have been possible to recover the electrostatic contribution from Eq. (58) in the $\beta \to 0$ limit.

lowing non-dimensional parameters:

$$kr_{c\epsilon}, \quad \frac{\omega}{\omega_{lh}}, \quad \frac{\gamma}{\omega_{lh}}, \quad \frac{T_i}{T_e}, \quad \frac{u_{de}}{v_{ti}},$$

$$\Psi, \quad \beta_e, \quad \frac{\omega_{pe}}{\omega_{ce}}, \quad \frac{m_i}{m_e}, \quad \frac{\nu_e}{\omega_{lh}}. \tag{65}$$

where $\omega_{lh} \simeq \sqrt{\omega_{ci}\omega_{ce}}$ is the lower hybrid frequency, β_e is the electron beta (ratio of electron thermal pressure to magnetic pressure), ω_{pe} is the electron plasma frequency and Ψ is related to the propagation angle θ (see Fig. (1)) scaled by the mass ratio

$$\Psi \equiv (m_e/m_i)^{1/2}\frac{k}{k_z} = \frac{(m_e/m_i)^{\frac{1}{2}}}{\cos\theta}. \tag{66}$$

The only lacking equation is one that relates the level of saturated microturbulence $\mathcal{E}_k/n_0T_i$ to the above parameters.

The formulation of this relation is, by far, the most formidable obstacle to the study of wave-particle transport, since such a relation must embody all the physics of the nonlinear saturation mechanism. The central question in this context concerns the mechanism through which the fluctuations, initiated by the instability, reach a steady-state. This mechanism dictates the magnitude and dependencies of the corresponding fluctuating energy density.

In this paper we shall adopt and compare four different saturation mechanisms: ion trapping, electron trapping, ion resonance broadening and thermodynamic bound. The models for each of these mechanisms are discussed in more detail in Ref. [4, pp.128-135]. For our purposes here we only quote the resulting expression for each of these saturation models.

4.1 Thermodynamic Limit: The Fowler Bound

An upper limit for $\mathcal{E}_t$ was first derived by *Fowler*[18] (1968) from thermodynamic arguments,

$$(\mathcal{E}_t)_{FB} \leq \frac{1}{2}n_e m_e u_{de}^2, \tag{67}$$

and simply states that the energy in the turbulent fields cannot exceed the kinetic energy of the electron drift that is fueling the instability. For a convenient incorporation in our particular formulation, we recast the inequality above to read

$$\frac{(\mathcal{E}_t)_{FB}}{n_oT_i} \leq \frac{m_e}{m_i}\left(\frac{u_{de}}{v_{ti}}\right)^2. \tag{68}$$

4.2 Saturation by Ion Trapping

In situations where the excited wave spectrum is narrow due to the dominance of a single wave mode, a monochromatic wave saturation model, such as that behind particle trapping, can prove to be a viable mechanism for saturation. In such a case the saturation dynamics can be governed by the trapping of the particles in the potential wells of the growing mode thus limiting its growth. At saturation one can simply write

$$e\tilde{\phi} = \frac{1}{2}m_i\left(\frac{\omega_r}{k}\right)^2 \tag{69}$$

where ω_r/k is the phase velocity of the dominant mode and we have assumed that the ions are the particles being trapped. Again, we normalize the saturation model for compatibility with transport theory so that, using $e\tilde{\phi} \approx e\tilde{E}/k$ and $\mathcal{E}_k = \epsilon_0|\tilde{E}_k|^2/2$, the above equation can be rewritten as

$$\frac{(\mathcal{E}_k)_{IT}}{n_oT_i} = \frac{1}{4\,(kr_{c\epsilon})^2}\left(\frac{\omega_{c\epsilon}}{\omega_{pe}}\right)^2\frac{T_e}{T_i}\left(\frac{\omega_r}{\omega_{lh}}\right)^4. \tag{70}$$

4.3 Saturation by Electron Trapping

Electron trapping is probably not a viable saturation mechanism for an instability in which electrons are collisional and are in broad-resonance with the unstable waves. We shall, however, include a model for electron trapping saturation in our calculations for the sake of reference. In analogy with ion trapping, we can write for the electrons as viewed from the ion rest frame

$$e\tilde{\phi} = \frac{1}{2}m_e\left(\frac{\omega_r}{k_z} - u_{de}\right)^2, \tag{71}$$

and after some algebraic manipulations,

$$\frac{(\mathcal{E}_k)_{ET}}{n_0T_i} = \frac{1}{4\,(kr_{c\epsilon})^2}\left(\frac{\omega_{c\epsilon}}{\omega_{pe}}\right)^2\frac{T_e}{T_i}\left[\Psi\frac{\omega_r}{\omega_{lh}} - kr_{c\epsilon}\frac{u_{de}}{v_{te}}\right]^4. \tag{72}$$

4.4 Saturation by Resonance Broadening

This mechanism relies on the broadening of wave-particle resonances by the random motion of particles in the turbulent electric field set-up by the micro-instability.

If resonance broadening is to be important in our case, it would most probably rely on ion dynamics, since the electrons are already broadly resonant

with the waves due to collisions and finite-beta effects while the ions are very narrowly-resonant[4].

Following *Gary* and *Sanderson*[19] who applied the *Dum-Dupree* resonance broadening formula[20] to the ions and found, after taking the velocity average $\int \Delta\omega f_{i_0}\, dv / \int f_{i_0}\, dv$,

$$(\mathcal{E}_k)_{IRB} = \frac{1}{2}\epsilon_0 B_0^2 \left(\frac{\omega_r}{k}\right)^2, \tag{73}$$

we specialize the ion resonance broadening model for our dimensionless parameters and obtain

$$\frac{(\mathcal{E}_k)_{IRB}}{n_0 T_i} = \frac{m_e/m_i}{(kr_{c_e})^2}\frac{T_e}{T_i}\left(\frac{\omega_{c_e}}{\omega_{p_e}}\right)^2\left(\frac{\omega_r}{\omega_{lh}}\right)^2. \tag{74}$$

5 Calculations of Anomalous Transport

Armed with the expressions for anomalous transport in Eqs. (61), (62) and (63) along with the tensor elements in Eqs. (87)-(94) (Appendix), the linear dispersion relation in Eq. (64), the transformations in Eqs. (47)-(57) and the saturation models in Eqs. (68), (70), (72), (74), we can now conduct a comparative numerical study of anomalous dissipation.

5.1 Classical Benchmarks

For benchmarks we shall use the following classical expressions for the momentum and energy exchange rates.

For the momentum exchange rate we take the classical Coulomb (electron-ion) collision frequency[10] for momentum relaxation $(\nu_e^p)_{CL}$

$$(\nu_e^p)_{CL} = \frac{n_e e^4 \ln\Lambda}{3(2\pi)^{3/2}\epsilon_0 m_e^{1/2} T_e^{3/2}} \tag{75}$$

where the plasma parameter Λ is given by

$$\Lambda = 9\left(\frac{4}{3}\right)\pi n_0 \lambda_{de}^3. \tag{76}$$

This collision frequency determines the classical Spitzer resistivity

$$(\eta)_{CL} = \frac{m_e (\nu_e^p)_{CL}}{n_0 e^2}. \tag{77}$$

For compatibility, we normalize with the lower hybrid frequency and cast the result in terms of our dimensionless parameters, to get

$$\frac{(\nu_e^p)_{CL}}{\omega_{lh}} = \frac{2}{\sqrt{2\pi}}\left(\frac{m_i}{m_e}\right)^{1/2}\frac{\omega_{p_e}}{\omega_{c_e}}\frac{\ln\Lambda}{\Lambda}. \tag{78}$$

For a heating rate benchmark we define a classical heating rate, $(\nu_e^T)_{CL}$, for Joule heating

$$(\nu_e^T)_{CL} \equiv \frac{1}{n_0 T_e}\frac{\partial}{\partial t} n_e T_e = \frac{2}{3}(\eta)_{CL}\frac{j^2}{n_0 T_e} \tag{79}$$

which yields

$$\begin{aligned}\frac{(\nu^T)_{CL}}{\omega_{lh}} &= \frac{8}{3\sqrt{2\pi}}\left(\frac{u_{de}}{v_{ti}}\right)^2\frac{T_i}{T_e}\left(\frac{m_e}{m_i}\right)^{1/2}\frac{\omega_{p_e}}{\omega_{c_e}}\frac{\ln\Lambda}{\Lambda} \\ &= \frac{4}{3}\left(\frac{u_{de}}{v_{ti}}\right)^2\frac{T_i}{T_e}\frac{m_e}{m_i}\frac{(\nu_e^p)_{CL}}{\omega_{lh}}.\end{aligned} \tag{80}$$

where the second equation shows the explicit dependence on the collision frequency.

Finally, we note that in calculating the anomalous rates we approximate the integrals, as commonly done in the literature, by the contribution of the dominant mode only (*i.e* for k^{**}), meaning that all the Fourier-decomposed properties are estimated at the doubly maximized growth (*i.e* maximized over wavelength and propagation angle)[3].

5.2 Numerical Results

Since β_e and u_{de}/v_{ti} are the two parameters that vary most within the plasma of the MPD thruster, they were chosen as the varying parameters of the calculations. When β_e is varied, u_{de}/v_{ti} is kept at 20, and when u_{de}/v_{ti} is varied, β_e is set at unity. The other parameters are $m_i/m_e = 73300$ (for argon), $T_i/T_e = 1$, $\nu_e/\omega_{lh} = 1$ and $\omega_{p_e}/\omega_{c_e} = 100$ for continuity with the calculations in Part II of our study[4].

5.2.1 Effects of Plasma Beta

The effects of plasma beta on the resistivity are shown in Fig. (2) where the ratio of anomalous to classical momentum exchange frequency (which is essentially the ratio of the corresponding resistivities (*cf* Eqs. (18) and Eq. (77)) is plotted versus beta for the parameters listed above. We immediately note

[3] Although this simplification is followed by almost all anomalous transport calculations in the literature, (often without justification) one must, for quantitative accuracy, check to see whether, indeed, the k-resolved rate calculations vary weakly with the wavenumber in the region of parameter-space of interest. Although we have done a few cursory checks on the sensitivity of the rates to the details of the spectrum we have not evaluated the above calculation method over a comprehensive range to warrant its accuracy over the entire plasma parameter range of interest, since we are only concerned here with order-of-magnitude variations in the rates. More accurate calculations in the future should address this question.

[4] Higher collisional rates will be considered in the MPD thruster-specific calculations of the next section.

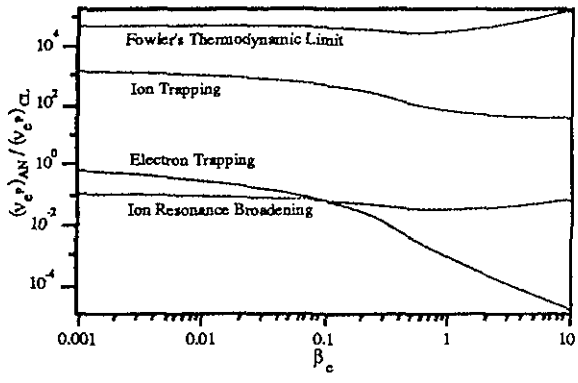

Figure 2: The anomalous momentum exchange frequency, $(\nu_e^p)_{AN}$, normalized by its classical counterpart and plotted versus the electron beta according to four saturation models. Argon with $u_{de}/v_{ti} = 20$, $T_i/T_e = 1$, $\nu_e/\omega_{lh} = 1$ and $\omega_{pe}/\omega_{ce} = 100$.

that, even when plotted on such a compacted logarithmic ordinate scale spanning eight orders of magnitude, all the curves can be seen to deviate from their $\beta_e \to 0$ asymptotes (which are practically reached at $\beta_e = .001$). These deviations are due to the electromagnetic corrections to the electrostatic limits, as separated in Eq. (58). We also note that the trapping models are most effected by finite-beta effects.

The ion trapping model is of special interest as discussed in Section 4.2 especially since it was the only one assumed in the purely electrostatic study of ref. [21]. We see that, when β_e is on the order of unity or greater, as is commonly the case of the MPD thruster plasma, the anomalous resistivity is an order of magnitude less than that predicted by the purely electrostatic limit.

The reason the anomalous resistivity decreases with increasing beta according to trapping models can be traced to the coupling with pseudo-whistler modes that we discussed in ref. [4]. As beta increases, the disturbances to the magnetic field do not have the time to dissipate (low Alfvén velocity) and significant electromagnetic coupling arises. The unstable waves acquire some of the characteristics of oblique whistlers and consequently the most unstable modes shift to lower frequencies. Since the saturation level due to trapping scales with frequency to the fourth power (*cf* Eq. (70)), the end effect is a substantial reduction in the anomalous resistivity.

It is relevant, in the context of a comparative study, to mention that a plausibility argument based on the concept of minimum dissipation is usually invoked in the literature when saturation mechanisms are compared. According to this argument the mechanism requiring the least energy at saturation is favored. A comparative analysis based solely on this criterion can, however, be misleading if it does not consider the viability of the physical mechanism independent of the global thermodynamics.

We note from the plot that the Fowler bound on the calculated rates allows, in principle, for a wide latitude for anomalous resistivity to be important.

We should not expect the electron trapping model to dictate the transport for arguments already made in previous sections. Furthermore, we should mention that more careful studies of resonance broadening than was made at the time the mechanism was first proposed, have shown that its effects are limited to a redistribution of energy in k-space at low plasma beta, and that it does not result in enough dissipation to saturate an instability (such as the case of the lower hybrid gradient driven instability (LHGDI), for instance) . Therefore, for low β_e, ion trapping is the most viable mechanism. At these conditions, the anomalous resistivity can be quite dominant (as is observed in Fig. (2)), more than two orders of magnitude larger than the classical value, in agreement with the findings of ref. [21]. As beta increases, saturation by resonance broadening can become more viable especially since the turbulent saturation levels are considerably lower than those for ion trapping (as is clear from the same plot). Whether one or the other mechanism controls saturation depends, at least partly, on whether the spectrum is narrow or broad. Even though experimental data on turbulent fluctuations in the MPD thruster[11, 3] give evidence of a dominant narrow (peaked) spectrum of turbulence in the lower hybrid range, the considerably lower levels of saturation energy implied by the ion resonance broadening mechanism warrant its consideration as a contender in the control of turbulent transport. Of course, this question is best answered by computer particle simulations.

If ion resonance broadening does take over the control of saturation, anomalous transport can, for the parameters in the above calculations, be brought down below classical levels. One should therefore expect, by virtue of the substantial variability of the plasma beta within the MPD thruster plasma, that there are regions where anomalous resistivity dominates over its classical analog as there are regions where the converse is true. More on this issue will be said in Section 5.3.

The same comments we made above also apply

for the anomalous electron heating rates that were normalized by the joule heating rate and plotted in Fig. (3). It is clear from this plot that when ion

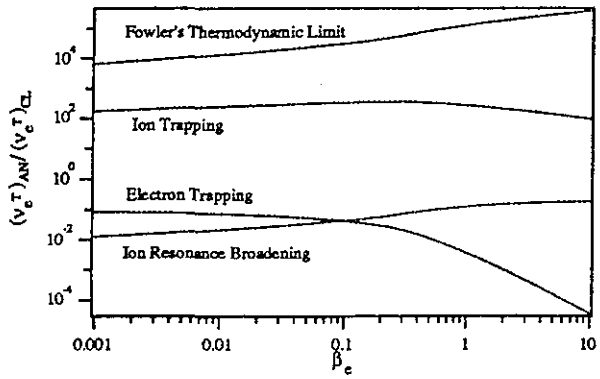

Figure 3: The anomalous electron heating rate, $\left(\nu_e^T\right)_{AN}$, normalized by the joule heating rate and plotted versus the electron beta according to four saturation models. Argon with $u_{de}/v_{ti} = 20$, $T_i/T_e = 1$, $\nu_e/\omega_{lh} = 1$ and $\omega_{pe}/\omega_{ce} = 100$.

trapping dominates, the anomalous heating rate is substantially larger than the electron joule heating rate. Ion heating rates are not shown here but were calculated in ref. [4] and were found to be similar in both magnitude and dependence as their electron counterparts.

To compare the two rates we have calculated their ratio and plotted the result in Fig. (4). There is only one curve in this figure because the various saturation models cancel out in the division. Since this ratio is independent of the saturation details, it is more accurate than the other quantities we have calculated. We note from this figure that, in the electrostatic limit, the two anomalous heating rates are basically equal. This feature is in contrast to the way electrons and ions are heated classically (especially for a heavy atom like argon) and is a well-known characteristic of the electrostatic LHCDI (or the modified two-stream instability, MTSI) as noted in ref. [22, 23]. Since the ions, are heated by the instability-induced turbulence at rates comparable to those of the electrons, and since in the MPD thruster, the electron energy is strongly tied to excitation and ionization through inelastic collisions, anomalous heating can offer an answer to the long standing question of why the ion temperature is somewhat higher than the electron temperature. Of course, for this argument to be true not only $\left(\nu_e^T\right)_{AN}$ must be comparable to $\left(\nu_i^T\right)_{AN}$, but the saturation level must be high enough to warrant the dominance of anomalous heating over classical heating. Such is the case when the instability saturates by trapping ions.

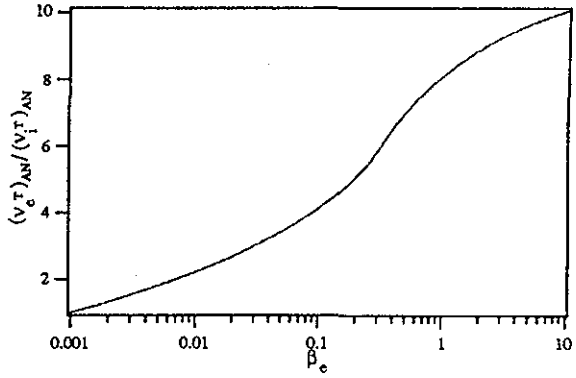

Figure 4: The anomalous electron heating rate, $\left(\nu_e^T\right)_{AN}$, normalized by the anomalous ion heating rate, $\left(\nu_i^T\right)_{AN}$, plotted versus the electron beta. Argon with $u_{de}/v_{ti} = 20$, $T_i/T_e = 1$, $\nu_e/\omega_{lh} = 1$ and $\omega_{pe}/\omega_{ce} = 100$.

The above argument about the relative temperatures is strongest in the electrostatic limit and is in agreement with ref. [21]. When electromagnetic effects start to become important with increasing beta, the same figure shows a degradation of the heating parity towards a progressively preferential heating of electrons. This finding is in agreement with that of ref. [16] where only the collisionless limit was studied. This degradation in heating parity is not strong enough, however, to weaken the grounds for the above argument concerning the relative temperatures, especially for a heavy atom like argon. Indeed, we see from the same figure that a four-octave increase in beta does not change the order of magnitude of the relative heating ratio.

The increase of preferential electron heating with increasing beta may be partly due to the fact that, at low beta, the instability has its dominant modes oriented at small angles to the magnetic field ($k_z/k \simeq (m_e/m_i)^{1/2}$ or $\Psi \simeq 1$) as was found in Part I of our study[1] and ref. [4], and consequently "perceives" the electron with an effective mass comparable to that of the ions[22]. As beta increases, electromagnetic coupling with oblique pseudo-whistlers cause the dominant modes to propagate more obliquely, as first noted by refs. [24] and [25] and extended by us, in ref. [4], to the collisional domain. Consequently, the effective electron mass decreases and the electrons be-

come much easier to heat than the ions.

5.2.2 Effects of the Drift Velocity

The effects of the drift velocity are illustrated in the plots of Figs. (5) and (6) for the same parameters as above but with β_e set to unity and u_{de}/v_{ti} varying between 10 and 100.

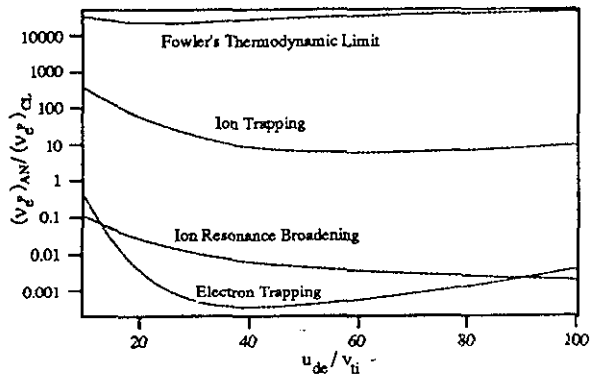

Figure 5: The anomalous momentum exchange frequency, $(\nu_e^p)_{AN}$, normalized by its classical counterpart and plotted versus the normalized drift velocity according to four saturation models. Argon with $\beta_e = 1$, $T_i/T_e = 1$, $\nu_e/\omega_{lh} = 1$ and $\omega_{pe}/\omega_{ce} = 100$.

In reference to Fig. (5) we note that the general decreasing trend of anomalous resistivity with the drift velocity, once the instability is onset[5], is not intuitive. One would expect that an increase in the free energy source of the instability would enhance the anomalous resistivity effect. In ref. [21] the same trend was found but no explanation was given.

This trend can be understood once we realize that the scaling of the linear growth rate of the dominant mode (which does increase with the drift velocity) does not *necessarily* reflect in weak turbulence (quasi-linear) transport scaling since the dependencies of the saturation mechanism (which is extraneous to linear theory) can overwhelm linear trends. This becomes clearer by noting that although an increase in the drift velocity does enhance the linear growth rate of the dominant mode as found in Part I of our study[1], it also shifts the modes to more oblique propagation and lowers their frequencies. Even though the instability goes to longer wavelength[4], the dependence of the saturation level for a trapping mechanism (*cf* Eq. (70)) scales with the frequency to the fourth power so that the frequency scaling of the saturation mechanism overpowers the growth scaling of the linear modes[6].

The Fowler bound, on the other hand, whose scaling is more strongly tied to the free energy source, does increase monotonically with the drift velocity, as seen from the resistivity plot.

As expected from the above beta-dependence study, anomalous electron heating rates exceed those of the ions for the present case of $\beta_e = 1$. The preferential electron heating is further enhanced by increasing drift velocity as can be seen in Fig. (6). The

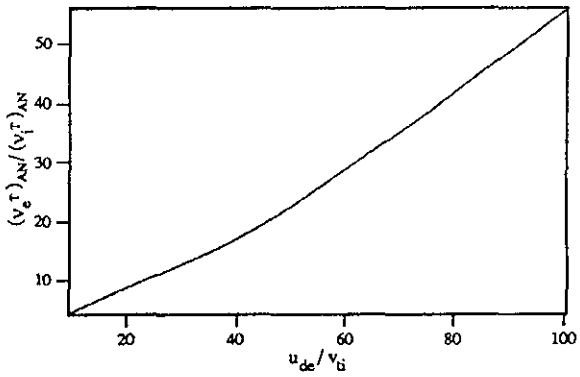

Figure 6: The anomalous electron heating rate, $(\nu_e^T)_{AN}$, normalized by the anomalous ion heating rate, and plotted for the same conditions as in Fig. (5).

reason for this behavior is similar to the one given above in the context of electromagnetic enhancement of electron preferential heating. This is so because both increasing beta and increasing drift velocity act to shift the instability toward more oblique propagation thus reducing the large $\bar{m}_e$-effect (where $\bar{m}_e$ is the effective electron mass that scales with the square of ψ) and subjecting the now "lighter" electrons to more heating.

5.3 MPD Thruster Calculations

We have, in the above calculations, chosen a set of parameters that is generally representative of the MPD

[5]The u_{de}/v_{ti} thresholds for the onset of the instability (start of positive linear growth) are not marked on these plots because they are on the order of unity.

[6]This trend is further accentuated for saturation by electron trapping because, in addition to the above arguments, the saturation level scales with Ψ^4 and Ψ decreases considerably (oblique propagation) with increasing drift velocity. At very high drift, the Doppler shift term in the saturation model (*cf* Eq. (72)) becomes more significant and reverts the trend, which explains the rise of the electron trapping curve in Fig. (5) at high values of u_{de}/v_{ti}.

thruster plasma. There is, however, one exception. It is the value of ν_e/ω_{lh} which we have set equal to unity as a compromise between having to represent a collisional plasma and providing a link with previous studies. Moreover, many of the complex interactions between the natural plasma modes, the free energy source and collisions are most pronounced when the collision frequency is on the order of the oscillating frequency. We now, supplement our calculations with results obtained at collisional levels more appropriate of the MPD thruster plasma.

In order to approximate a typical range for MPD thruster plasma collisionality, we consider the typical range for the variation of temperature and density. For more detail on how the various parameters of interest vary within the MPD thruster discharge the reader is referred to the recent parameter review in ref. [11]. Assuming that T_e varies between 1.5 and 3 eV, while n_0 ranges between 10^{20} and 1.5×10^{22} m^{-3}, we can calculate a lower and upper bound for ν_e/ω_{lh} in argon from Eq. (78) to be 25 and 500, respectively, where we have fixed ω_{pe}/ω_{ce} at 100 for compatibility with the above calculations.

For the results shown in Fig. (7) we have chosen to fix beta at unity to preserve electromagnetic effects and varied u_{de}/v_{ti} from 100 down to the threshold of the instability, which, although slightly exaggerated in the figure, was at $u_{de}/v_{ti} \simeq 1.5$. For each of the three considered mechanisms the plot shows a band whose upper line corresponds to the moderately collisional condition $\nu_e/\omega_{lh} = 25$ ($T_e = 3$ eV, $n_0 = 10^{20}$ m^{-3}) and whose lower (broken) line corresponds to the strongly collisional condition $\nu_e/\omega_{lh} = 500$ ($T_e = 1.5$ eV, $n_0 = 1.5 \times 10^{22}$ m^{-3}).

The trends in this plot are similar to those already illustrated in Fig. (5) which indicated that we have not jeopardized any physics by assuming $\nu_e/\omega_{lh} = 1$ previously.

We note from the figure that, although the Fowler bound allows for a large microturbulent contribution to the resistivity, ion resonance broadening might cause the instability to saturate at low levels. Even though arguments have been advanced recently discounting the effectivity of such a mechanism, it should not be totally discounted pending strong evidence from computer particle simulations and/or dedicated experiments.

We furthermore see that, in the case of ion trapping saturation, once the instability is onset, the importance of anomalous resistivity in the MPD thruster plasma is not as much dictated by the drift velocity (since the two limiting curves are quite flat), as

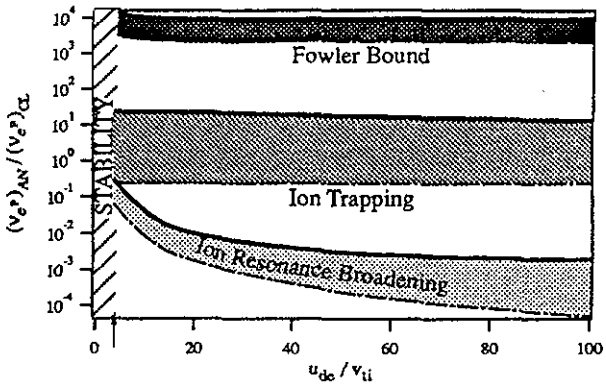

Figure 7: The anomalous momentum exchange frequency, $(\nu_e^p)_{AN}$, normalized by its classical counterpart and plotted versus the normalized electron drift velocity according to three saturation models. The upper line of each band corresponds to the moderately collisional condition $\nu_e/\omega_{lh} = 25$ ($T_e = 3$ eV, $n_0 = 10^{20}$ m^{-3}) and the lower (broken) line corresponds to the strongly collisional condition $\nu_e/\omega_{lh} = 500$ ($T_e = 1.5$ eV, $n_0 = 1.5 \times 10^{22}$ m^{-3}). Argon with $\beta_e = 1$, $T_i/T_e = 1$, and $\omega_{pe}/\omega_{ce} = 100$.

one would intuitively suspect, as it is dictated by the level of collisionality. Indeed, if collisionality is strong, anomalous resistivity can be kept below classical levels even if the instability is excited and even if ion trapping is responsible for saturation, as is clear from the plot[7]. This implies that low density regions of the MPD thruster discharge, such as regions depleted from charge due to the $j_z B_\theta$ Lorentz force component, tend to be more vulnerable to anomalous resistivity than denser (or more collisionally dominated) regions. This trend is in agreement with the well-known fact that dissipation in charged-depleted regions of the device, like the anode vicinity[26], is enhanced by weak collisionality.

Stated differently, under MPD thruster plasma conditions and for the microinstabilities in question, the level of anomalous contribution to resistivity is dictated to a large extent by the parameter ν_e/ω_{lh}. It is interesting to note that this parameter is directly related to the electron Hall parameter Ω_{H_e}. Indeed, it is just the inverse of the electron Hall parameter

[7]It must be said, however, that even in the case of high collisionality ($\nu_e/\omega_{lh} \simeq 500$) where anomalous resistivity is kept below classical levels, it is still a finite fraction of its classical counterpart (about 25% in the above calculations), as can be seen from the same plot (again, assuming ion trapping saturation).

scaled by the square root of the mass ratio

$$\Omega_{H_e} \equiv \frac{\omega_{ce}}{\nu_e} = \frac{(m_i/m_e)^{1/2}}{\nu_e/\omega_{lh}}. \quad (81)$$

The known scaling of the anode voltage drop with the Hall parameter (see for instance the recent measurements in ref. [26]) that constitutes one of the most dissipative sinks for the low-power MPD thruster is thus another invariant behavioral trait of the accelerator that could possibly be explained by the effects of microinstabilities.

The anomalous ion and electron heating rates were also calculated in ref. [4] and found to have the same general trends as those of the anomalous resistivity.

6 Anomalous Transport Models for Inclusion in Fluid Codes

A spatial resolution of the realms of anomalous and classical transport within the MPD thruster discharge and their dependence on the accelerator's operating conditions can only be addressed accurately with an improved fluid code that incorporates the above theories in a self-consistent fluid-kinetic description. This may be accomplished by carrying *a priori* calculations of the relevant anomalous transport for the expected parameter-space covered by typical numerical simulations then fitting the calculations with polynomial expressions. These expressions become the transport models suitable for inclusion in codes for the self-consistent numerical simulation of MPD thruster flows.

In general the microstability (and hence microturbulence) description depends on the following set of eight independent macroscopic parameters

$$kr_{ce}, \quad \Psi, \quad \frac{m_i}{m_e}, \quad \frac{\omega_{pe}}{\omega_{ce}}, \quad \beta_e, \quad \frac{u_{de}}{v_{ti}}, \quad \frac{T_i}{T_e}, \quad \Omega_{H_e} \quad (82)$$

(where T_i is the same as T_h in the flow code). The first two parameters kr_{ce} (r_{ce} being the electron cyclotron radius) and Ψ represent the normalized wavenumber and propagation angle (with respect to the magnetic field) of the oscillations respectively and are varied to growth-maximize the solutions. Since all anomalous transport rates used here were calculated at maximum growth these two parameters drop out of the final models. The mass ratio m_i/m_e is that of argon. All solutions were found to be very insensitive to the fourth parameter, namely the ratio of electron plasma frequency to the electron cyclotron frequency ω_{pe}/ω_{ce}, as long as that ratio exceeded 10 which was the case for the simulations conducted so far[5, 6]. Similarly, the solutions were weakly dependent on β_e (the ratio of electron thermal pressure to magnetic pressure) as long as the electron Hall parameter did not exceed 10. Although that was the case for the numerical simulations in Refs. [5, 6], it is expected that the simulation of more realistic geometries at high total currents would raise the electron Hall parameter enough to require the full inclusion of finite-beta effects.

The last three parameters are the most important for our problem. First, u_{de}/v_{ti} must reach a threshold for the instability to be excited and hence for anomalous transport to be operative. For the entire region of the investigated parameter-space that threshold was very near 1.5. Second, the ion to electron temperature ratio plays a role in scaling the level of turbulence. Invariably for our parameter-space, it was found that increasing T_i/T_e causes a devaluation of anomalous transport. The most important of all the macroscopic parameters turned out to be the last one namely the electron Hall parameter Ω_{H_e}.

The anomalous resistivity η_{AN}

$$\eta_{AN} \equiv \frac{m_e(\nu_e)_{AN}}{e^2 n_e}, \quad (83)$$

calculated using the theory presented in the above sections, and normalized by its classic counterpart $\eta_{Cl} \equiv m_e\nu_e/e^2n_e$ is shown in Fig. (8). It is important to note that an increase in the electron Hall parameter for typical values of T_i/T_e leads to a very significant increase in the anomalous resistivity *if* the parameter u_{de}/v_{ti} is above the stability threshold. It is interesting to note that the scaling of this ratio with the Hall parameter is in general agreement with that recently inferred by Gallimore[27] from measurements in the anode region.

A similar plot is shown in Fig. (9) for the ion heating rate $(\nu_i^T)_{AN}$ normalized by the Coulomb frequency.

A two-parameter, variable cross-term, least square fit was made to the calculated rates shown in Figs. (8) and (9) in order to make them suitable for inclusion in plasma fluid flow codes.

The resulting two-parameter interpolating polynomial for $(\nu_i^T)_{AN}/\nu_{ei}$ has an average accuracy of 15% and reads

$$\frac{(\nu_i^T)_{AN}}{\nu_{ei}} = 5.36 \times 10^{-5} + 1.29 \times 10^{-5}\ \Omega$$

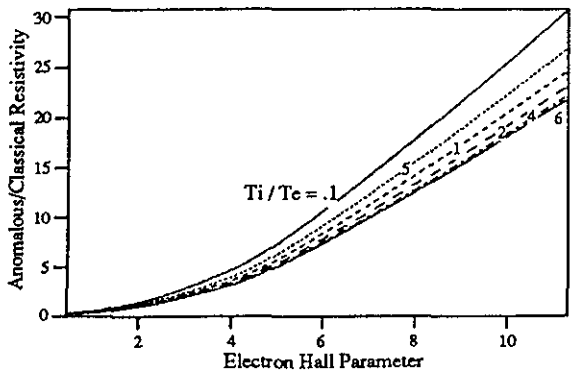

Figure 8: Ratio of anomalous resistivity to classical resistivity as a function of the electron Hall parameter and T_i/T_e with u_{de}/v_{ti} exceeding 1.5,

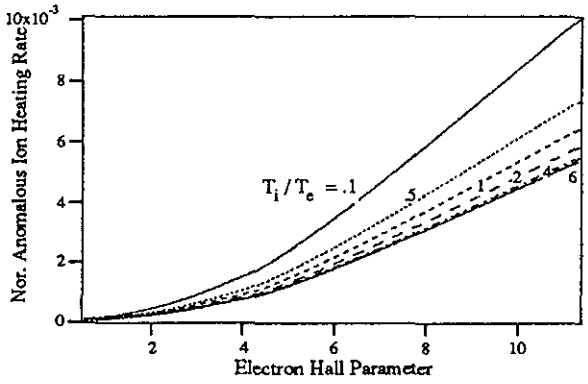

Figure 9: Anomalous ion heating rate normalized by the Coulomb frequency as a function of the electron Hall and T_i/T_e with u_{de}/v_{ti} exceeding 1.5

$$+ 6.03 \times 10^{-6}\ \Omega^2 + 9.44 \times 10^{-8}\ \Omega^3 + \frac{T_h}{T_e}(-7.55 \times 10^{-7} - 5.41 \times 10^{-6}\ \Omega - 3.93 \times 10^{-6}\ \Omega^2). \quad (84)$$

The ions are heated by the turbulent fluctuations at a rate $(Q_i)_{AN} = \frac{3}{2}(\nu_i^T)_{AN} T_h$

The effective conductivity introducing the anomalous resistivity effect to the flow code has the form

$$\sigma_{eff} = \frac{e^2 n_e}{m_e(\nu_{ei} + (\nu_e^P)_{AN})}, \quad (85)$$

where $(\nu_e^P)_{AN}$ is the electron-wave momentum exchange frequency, which is again computed through an interpolating polynomial of average accuracy of 10%

$$\frac{(\nu_e^P)_{AN}}{\nu_{ei}} = 0.192 + 3.33 \times 10^{-2}\ \Omega + .212\Omega^2 - 8.27 \times 10^{-5}\ \Omega^3 + \frac{T_h}{T_e}(1.23 \times 10^{-3} - 1.58 \times 10^{-2}\ \Omega - 7.89 \times 10^{-3}\ \Omega^2). \quad (86)$$

The use of these models in fluid code may proceed in the following way. At all the gridpoints where $u_{de}/v_{ti} < 1.5$ both, $(\nu_e^P)_{AN}$ and $(\nu_i^T)_{AN}$ are set to zero and all transport is assumed purely classical. Otherwise, the anomalous rates are computed from the above polynomials using the instantaneous macroscopic parameters and folded back into the flow equations at every time step thus insuring self-consistency.

7 Conclusions and Final Remarks

Using plasma weak turbulence theory, a second order model of wave-particle transport and anomalous dissipation was developed for the plasma of the MPD accelerator. The model was also based on the linear kinetic description of instabilities in a magnetoactive, collisional, finite-beta, current-carrying and flowing plasma developed in Part II of our study[2]. Assuming ion trapping to be the saturation mechanism, as it is most likely the case, our calculations show that the saturation of the finite-beta lower hybrid current drift instability (LHCDI), which has been observed in the MPD thruster plasma, can cause a severe enhancement to the local resistivity and the bulk heating rate of both ions and electrons. It can also cause a preferential effective heating of the ions and enhance both heating and resistivity in regions of low collisionality (High electron Hall parameters) such as near the anode. The resulting microturbulence thus offers a possible explanation for many hitherto unsettled questions about the MPD thruster. What is the nature of thermal dissipation limiting the efficiency? Why does the ion temperature exceed that of the electrons? What is the nature of the anode drop? Why does the anode drop scale with the electron Hall parameter? These are some of the questions that have been answered, at least partly, through the study of the physics and dependencies of microturbulence. More problems, such as the spatial location of the regions most affected by anomalous trans-

port in the MPD thruster discharge, and the effects of geometry and operation conditions, can best be studied with fluid codes that include self-consistently these microturbulent effects. Towards this end, we have also presented polynomial models for the relevant anomalous transport suitable for inclusion in such codes.

Another important problem that still needs to be modeled more carefully is the very likely role of microturbulence in ionization. This problem has been rendered more urgent by the recent spectroscopic study of *Randolph et al.*[28] that confirmed our 1985 speculations[29] on the importance of microinstability-driven ionization.

References

[1] E.Y. Choueiri, A. J. Kelly, and R. G. Jahn. Current-driven plasma acceleration versus current-driven energy dissipation part I : Wave stability theory. In 21^{st} *International Electric Propulsion Conference*, Orlando, Florida, 1990. AIAA-90-2610.

[2] E.Y. Choueiri, A. J. Kelly, and R. G. Jahn. Current-driven plasma acceleration versus current-driven energy dissipation part II : Electromagnetic wave stability theory and experiments. In 22^{nd} *International Electric Propulsion Conference*, Viareggio, Italy, 1991. IEPC-91-100.

[3] D.L. Tilley, E.Y. Choueiri, A.J. Kelly, and R.G. Jahn. An investigation of microinstabilities in a kW level self-field MPD thruster. In 22^{nd} *International Electric Propulsion Conference*, Viareggio, Italy, 1991. IEPC-91-122.

[4] E.Y. Choueiri. *Electron-Ion Streaming Instabilities of an Electromagnetically Accelerated Plasma.* PhD thesis, Princeton University, Princeton, NJ, USA, 1991.

[5] G. Caldo, E.Y. Choueiri, A. J. Kelly, and R. G. Jahn. An MPD code with anomalous transport. In 22^{nd} *International Electric Propulsion Conference*, Viareggio, Italy, 1991. IEPC-91-101.

[6] G. Caldo, E.Y. Choueiri, A. J. Kelly, and R. G. Jahn. Numerical simulation of MPD thruster flows with anomalous transport. In 28^{th} *Joint Propulsion Conference*, Nashville, TN, 1992. AIAA-92-3738.

[7] A.A. Vedenov, E.P. Velikhov, and R.Z. Sagdeev. Theory of a weakly turbulent plasma. *Nuclear Fusion*, 1:82–100, 1961.

[8] W.E. Drummond and M.N. Rosenbluth. Anomalous diffusion arising from microinstabilities in a plasma. *Physics of Fluids*, 5(12):1507–1513, 1962.

[9] A.A. Galeev and R.Z. Sagdeev. Theory of weakly turbulent plasma. In A.A. Galeev and R.N. Sudan, editors, *Basic Plasma Physics II.* North-Holland Physics Publishing, Amsterdam, 1984. Part 4.

[10] D.G. Swanson. *Plasma Waves.* Academic Press, Inc., San Diego, 1989.

[11] D.L. Tilley. An investigation of microinstabilities in a kW level self-field MPD thruster. Master's thesis, Princeton University, Princeton, NJ, USA, 1991.

[12] R.C. Davidson and N.A. Krall. Anomalous transport in high-temperature plasmas with applications to solenoidal fusion systems. *Nuclear Fusion*, 17(6):1313–1372, 1977.

[13] K. Papadopoulos. Microinstabilities and anomalous transport. In R.G. Stone and B.T. Tsurutani, editors, *Collisionless Shocks in the Heliosphere: A Tutorial Review.* American Geophysical Union, Washington, DC, 1985.

[14] R.C. Davidson. *Methods in Nonlinear Plasma Theory.* Academic Press, Inc., New York, 1972.

[15] E.M. Lifshitz and L.P. Pitaevskii. *Statistical Physics, 3^{rd} Edition, Part 1.* Pergamon Press, Oxford, 1980.

[16] D. Winske, M. Tanaka, C.S. Wu, and K.B. Quest. Plasma heating at collisionless shocks due to the kinetic cross-field streaming instability. *Journal of Geophysical Research*, 90(A1):123–136, 1985.

[17] D. Winske, 1991. Los Alamos Natinal Laboratory. Personal communication.

[18] T.K. Fowler. Thermodynamics of unstable plasmas. In A. Simon and W.B. Thompson, editors, *Advances in Plasma Physics*, pages 201–226. Interscience Publishers, New York, 1968.

[19] S.P. Gary and J.J. Sanderson. Energy transport by weak electrostatic drift fluctuations. *Physics of Fluids*, 24(4):638–650, 1981.

[20] C.T. Dum and T.H. Dupree. Nonlinear stabilization of high-frequency instabilities in a magnetic field. *The Physics of Fluids*, 13(8):2064–1081, 190.

[21] D. Hastings and E. Niewood. Theory of the modified two stream instability in an MPD thruster. In 25^{th} *Joint Propulsion Conference*, Monterey, CA, USA, 1989. AIAA-89-2599.

[22] J.B. McBride, E.Ott, J.P. Boris, and J.H. Orens. Theory and simulation of turbulent heating by the modified two-stream instability. *Physics of Fluids*, 15(12):2367–2383, 1972.

[23] J.B. McBride and E. Ott. Electromagnetic and finite-β_e effects on the modified two stream instability. *Physics Letters*, 39A(5):363–364, 1972.

[24] C.S. Wu, Y.M. Zhou, S.T. Tsai, and S.C. Guo. A kinetic cross-field streaming instability. *Physics of Fluids*, 26(5):1259–1267, 1983.

[25] S.T. Tsai, M. Tanaka, J.D. Gaffey Jr., E.H. Da Jornada, and C.S. Wu. Effect of electron thermal anisotropy on the kinetic cross-field streaming instability. *Journal of Plasma Physics*, 32(1):159–178, 1984.

[26] A.D. Gallimore. Thruster anode processes. Contribution to the March/April Bimonthly Progress Report of the Electric Propulsion and Plasma Dynamics Laboratory. Technical Report MAE 1776.30, Electric Propulsion and Plasma Dynamics Laboratory, Princeton University, 1991.

[27] A.D. Gallimore, A. J. Kelly, and R. G. Jahn. Anode power deposition in MPD thrusters. In 22^{nd} *International Electric Propulsion Conference*, Viareggio, Italy, 1991. IEPC-91-125.

[28] T.M. Randolph, W.F. Von Jaskowsky, A. J. Kelly, and R. G. Jahn. Measurement of ionization levels in the interelectrode region of an MPD thruster. In 28^{th} *Joint Propulsion Conference*, Nashville, TN, 1992. AIAA-92-3460.

[29] E.Y. Choueiri, A.J. Kelly, and R.G. Jahn. The manifestation of Alfvén's hypothesis of critical ionization velocity in the performance of MPD thrusters. In 18^{th} *International Electric Propulsion Conference*, Alexandria, Virginia, USA, 1985. AIAA-85-2037.

Appendix

The elements of the dispersion tensor D_{ij} needed for the above calculations were derived in Part II of our study[2] and are quoted here for the sake of completeness.

$$D_{11} = 1+\alpha_i(1+\zeta_i Z_i) + \alpha_e\left(\frac{1+\zeta_{e0}e^{-\mu_e}\sum_{n=-\infty}^{\infty} I_n Z_{en}}{1+i(\nu_e/k_z v_{te})e^{-\mu_e}\sum_{n=-\infty}^{\infty} I_n Z_{en}}\right) \quad (87)$$

$$D_{12} = -i\frac{\omega_{pe}^2}{\tilde{\omega}^2}\frac{k_z}{k}\zeta_{e0}\sqrt{2\mu_e}e^{-\mu_e} \times \sum_{n=-\infty}^{\infty}(I_n - I_n')(1+\tilde{\zeta}_{e0}Z_{en}) \quad (88)$$

$$D_{13} = 2\frac{\omega_{pe}^2}{\tilde{\omega}^2}\frac{k_z}{k}\zeta_{e0}e^{-\mu_e} \times \sum_{n=-\infty}^{\infty} I_n\left\{\vartheta_n^2 Z_{en} + \left[\left(\frac{u_{de}}{v_{te}}\right)^2/\zeta_{e0}\right] + (1+\zeta_{en}Z_{en})\left(\vartheta_n\frac{k_\perp^2 - k_z^2}{k_\perp k_z} - \zeta_{en}\right)\right\} \quad (89)$$

$$D_{22} = 1 - N^2 + \frac{\omega_{pi}^2}{\omega^2}\zeta_i Z_i + \frac{\omega_{pe}^2}{\tilde{\omega}^2}\zeta_{e0}\mu_e e^{-\mu_e} \times \sum_{n=-\infty}^{\infty}\left[\frac{n^2}{\mu_e^2}I_n + 2(I_n - I_n')\right]Z_{en} \quad (90)$$

$$D_{23} = -i\frac{\omega_{pe}^2}{\tilde{\omega}^2}\zeta_{e0}\sqrt{2\mu_e}e^{-\mu_e}\sum_{n=-\infty}^{\infty}(I_n - I_n') \times \left[1+\left(\frac{k_z}{k_\perp}\vartheta_n + \zeta_{en}\right)Z_{en}\right] \quad (91)$$

$$D_{33} = 1 - N^2 + \frac{\omega_{pi}^2}{\omega^2}\zeta_i Z_i + 2\frac{\omega_{pe}^2}{\tilde{\omega}^2}\frac{k_\perp^2}{k^2}\left[\left(\zeta_{e0} - \frac{k_z}{k_\perp}\frac{u_{de}}{v_{te}}\right)^2 + \zeta_{e0}e^{-\mu_e} \times \sum_{n=-\infty}^{\infty} I_n Z_{en}\left(\frac{k_z}{k_\perp}\vartheta_n + \zeta_{en}\right)^2\right] \quad (92)$$

$$D_{21} = -D_{12}; \quad D_{31} = \frac{k_\perp^2}{k^2}D_{13} \quad (93)$$

$$D_{32} = -\frac{k_\perp^2}{k^2} D_{23} \tag{94}$$

where I_n is the modified Bessel function of the first kind of order n and where we have used the following definitions

$$\zeta_{en} \equiv \frac{\omega + n\omega_{ce} - k_\perp u_{de} + i\nu_e}{k_z v_{te}}; \quad \zeta_i \equiv \frac{\omega - k_\perp u_f}{k v_{ti}}; \tag{95}$$

$$\tilde{\omega} \equiv \omega + i\nu_e; \quad \tilde{\zeta}_{e0} \equiv \frac{\tilde{\omega}}{k_z v_{te}} = \zeta_{e0} + \frac{k_\perp}{k_z}\frac{u_{de}}{v_{te}}; \tag{96}$$

$$\vartheta_n \equiv \frac{k_z}{k_\perp}(\zeta_{en} - \tilde{\zeta}_{e0}); \; Z_{en} \equiv Z(\zeta_{en}); \; I_n \equiv I_n(\mu_e). \tag{97}$$

where Z is the standard plasma dispersion function and where the thermal velocity, plasma frequency and cyclotron frequency of species s are, respectively, given by

$$v_{ts} = (2T_s/m_s)^{1/2}; \; \omega_{ps} \equiv \left(\frac{q_s^2 n_{0_s}}{\epsilon_0 m_s}\right)^{1/2}; \; \omega_{cs} \equiv \frac{q_s B_0}{m_s}. \tag{98}$$